The International Journal of Advanced Manufacturing Technology (2022) 120:265–277
https://doi.org/10.1007/s00170-022-08705-3

ORIGINAL ARTICLE

A hybrid multi-step method based on 1/3 and 3/8 Simpson formulas for milling stability prediction

Danian Zhan[1] · Shanglei Jiang[1] · Shikang Li[1] · Yuwen Sun[1]

Received: 7 October 2021 / Accepted: 6 January 2022 / Published online: 31 January 2022

Abstract
Chatter is an unfavorable phenomenon frequently experienced in the milling process, which severely reduces machining productivity and surface quality. The prediction of milling stability is essential for realizing chatter-free machining. This paper presents a hybrid multi-step method to predict the milling stability. Firstly, the milling dynamic system including regenerative effect is described as time-periodic delay differential equations (DDEs) that are then re-expressed as state-space equations. Secondly, the time period is divided into free vibration duration and forced vibration duration. With the forced vibration duration being divided into small time intervals, the integral response is approximated by hybrid multi-step Simpson formulas, where the fourth state item is approximated by the 3/8 Simpson formula and the remaining state items are approximated by the 1/3 Simpson formula. Finally, the Floquet transition matrix over the time period is constructed by a linear discrete map, and the milling stability is predicted via the Floquet theory. By using the benchmark examples from literatures, the convergence rates and stability boundaries of the proposed method are compared with typical methods, such as the updated numerical integration method (UNIM) and the fourth-order full-discretization method (4th FDM). Numerical results show that the proposed method can achieve high stability prediction accuracy with high efficiency. Furthermore, a series of milling experiments are carried out to verify the reliability and feasibility of the proposed method. According to the waveform and spectrum analysis of lots of synchronously measured sound and displacement signals, it can be found that the predicted stability boundaries are in good agreement with the experimental results.

Keywords Chatter · Milling stability · Hybrid multi-step method · Simpson formulas · Floquet theory

1 Introduction

Chatter is still the main limitation in achieving high-performance machining [1]. It easily occurs due to the flexibility of the milling system, which leads to poor surface quality, low machining productivity and reduced tool life, even causes damage to the machine tool spindle. The dynamic milling process can be formulated as delay differential equations (DDEs) with time-periodic coefficients [2, 3]. Based on stability analysis of the time-periodic DDEs, chatter can be effectively avoided by constructing the stability lobe diagram (SLD). Various methods including time domain methods, frequency domain methods, and discrete time domain methods have been proposed.

The time domain methods are the earliest methods for predicting the milling stability, which obtain the time domain dynamic response by solving the initial value problem of the DDEs, and then determine the stability according to the variation trend of the response. Smith and Tlusty [4] developed a time domain simulation method to generate the SLD for the milling process, in which the PTP (peak-to-peak) diagrams are outlined for the evaluation of the simulation results of multiple runs. Campomanes and Altintas [5] presented an improved time domain model to simulate the dynamic milling at low radial immersions. Although time domain simulations have the advantage of dealing with complex nonlinear effects in milling processes, its computational efficiency is relatively low. Based on the mean of the time-periodic coefficients, Altintas and Budak [6] proposed the well-known zero-order approximation (ZOA) method in the frequency domain, which can achieve the analytic prediction

✉ Shanglei Jiang
sljiang@dlut.edu.cn

✉ Yuwen Sun
ywsun@dlut.edu.cn

[1] Key Laboratory for Precision and Non-Traditional Machining Technology of the Ministry of Education, Dalian University of Technology, Dalian 116024, China

of milling stability. Its prediction accuracy is easily guaranteed at large radial immersions, but for the highly intermittent milling processes with small radial immersion, it will lead to unacceptable results [2, 7]. To overcome this issue, Budak and Altintas [8] and Merdol and Altintas [9] developed the multi-frequency solution (MFS) methods by taking the higher-order harmonics of time-periodic coefficients into account, which obtained improved prediction for the milling processes with small radial immersions.

Many discrete time domain methods are also studied especially in recent years. The key idea of discrete time domain methods is to convert the original DDEs to the state space and divide the tooth passing period equally into many small time intervals. Then these methods construct the Floquet transition matrix over one discrete time period, and finally judge the stability via the Floquet theory. Insperger and Stépán [10, 11] proposed the well-accepted semi-discretization method (SDM) and first-order semi-discretization method (1st SDM) for milling stability prediction, in which the delay term of DDEs in state space was approximated respectively by zeroth-order and first-order piecewise constant function. Furthermore, the convergence rates of the two SDMs were carefully investigated in detail in Ref. [11]. After that, some researchers expanded the two SDMs to predict the stability of various complex milling processes [12–14]. It should be noted that during the numerical calculation of the two SDMs, a lot of matrix inversion and matrix exponential computations are required. To some extent, this will reduce the computational efficiency. To handle this issue, Jiang et al. [15] adopted the improved precise time-integration algorithm (PTI) to compute exponential matrices and developed a second-order SDM (2nd SDM) for stability prediction of the milling system. Recently, they extended this method to predict the stability of thin-walled part milling [16] and five-axis ball-end milling with variable pitch cutter [17]. Based on the direct integration scheme, Ding et al. [18] proposed the full-discretization method (FDM). Compared with SDMs, both the state term and the delay term are approximated by linear interpolations in FDM, which improves the computational speed. To improve the computational accuracy of FDM, many higher-order versions of FDM based on high-order interpolation or approximation theory were put forward, such as the second-order FDM (2nd FDM) [19], the third-order FDM (3rd FDM) [20, 21], the hyper-third FDM [22], and the fourth-order FDM (4th FDM) [23]. Ozoegwu [23] pointed out that with increasing interpolation orders, the computational accuracy of FDM may not be always improved.

Bayly et al. [24] divided the tooth passing period into free vibration duration and forced vibration duration separately. They suggested the temporal finite element analysis method (TFEM) to predict the milling stability, which can achieve accurate predictions especially at small radial immersions. Ding et al. [25] divided the forced vibration time into small intervals and transformed the time-periodic DDEs into integral equations. On this basis, they proposed several efficient numerical integration methods (NIMs) based on different numerical integration formulas. Xia et al. [26] presented an improved numerical integration method based on the Lagrange interpolation scheme. Zhang et al. [27] developed a varying-step NIM to calculate the stability lobes of unequal-pitch cutters. Under the same framework of NIM, Niu et al. [28] proposed the generalized Runge–Kutta method (GRKM) with a higher convergence rate. Zhang et al. [29] presented a compact Simpson method for stability prediction, which can save more computational time. They claimed that the local discretization error of the Simpson method was $O\left(h^5\right)$ at first, but soon published a corrigendum modifying it into $O\left(h^3\right)$. This is because the trapezoidal rule is utilized at time point $t = t_2$ when constructing the periodic discrete dynamic map, but the local discretization error of the trapezoidal rule was $O\left(h^3\right)$. Dong and Qiu [30] proposed the updated numerical integration method (UNIM) based on Hermite numerical integration and its effectiveness was verified by milling experiments. Li et al. [31] suggested the Newton–Cotes method. Later, Wang et al. [32] extended this method to predict the stability of the milling system with multiple modes. In addition to the above methods, some other methods [33, 34] from discrete time domain are also proposed to continue to improve the calculation performance.

In this paper, a hybrid multi-step method based on 1/3 and 3/8 Simpson formulas is presented to achieve accurate stability prediction of milling processes with a significantly improved convergence rate. The fourth state item and the remaining state items are respectively approximated by the 3/8 Simpson formula and the 1/3 Simpson formula, which can overcome the decreasing order of local discretization error due to the application of the trapezoidal rule in literature. Only the Simpson formulas are used in the proposed method, which not only ensures efficient computation, but also improves the prediction accuracy of SLDs. The remainder of this paper is organized as follows. Section 2 presents the mathematical model of milling dynamics and the hybrid multi-step method. Section 3 shows the convergence rate and prediction accuracy of the proposed method. Section 4 validates the proposed method via milling experiments. Some conclusions are drawn in Sect. 5.

2 Mathematical model and algorithm

In general, the mathematical model of milling dynamics considering the regenerative effect can be described as [2, 35]:

$$\mathbf{M}\ddot{\mathbf{q}}(t)+\mathbf{C}\dot{\mathbf{q}}(t)+\mathbf{K}\mathbf{q}(t)=-a_p\mathbf{K}_c(t)\left[\mathbf{q}(t)-\mathbf{q}(t-\tau)\right] \tag{1}$$

where $\mathbf{M}$, $\mathbf{C}$, $\mathbf{K}$, and $\mathbf{q}(t)$ represent the modal mass matrix, the modal damping matrix, the modal stiffness matrix, and the modal displacement vector, respectively. a_p denotes the axial depth of cut. τ is the tooth passing period that can be calculated by $\tau=60/(\Omega N)$, where Ω represents the spindle speed (rpm) and N represents the number of cutter teeth. $\mathbf{K}_c(t)$ represents the time-periodic coefficient matrix, satisfying $\mathbf{K}_c(t)=\mathbf{K}_c(t+\tau)$.

By state space transformation with $\mathbf{p}(t)=\mathbf{M}\dot{\mathbf{q}}(t)+\mathbf{C}\mathbf{q}(t)/2$ and $\mathbf{X}(t)=\begin{bmatrix}\mathbf{q}(t)\\ \mathbf{p}(t)\end{bmatrix}$, Eq. (1) can be rewritten in the state-space form:

$$\dot{\mathbf{X}}(t)=\mathbf{A}\mathbf{X}(t)+\mathbf{B}(t)[\mathbf{X}(t)-\mathbf{X}(t-\tau)] \tag{2}$$

where $\mathbf{A}=\begin{bmatrix}-\mathbf{M}^{-1}\mathbf{C}/2 & \mathbf{M}^{-1}\\ \mathbf{C}\mathbf{M}^{-1}\mathbf{C}/4-\mathbf{K} & -\mathbf{C}\mathbf{M}^{-1}/2\end{bmatrix}$, $\mathbf{B}(t)=\begin{bmatrix}0 & 0\\ -a_p\mathbf{K}_c(t) & 0\end{bmatrix}$.

Based on the direct integration scheme [25], the analytical solution of Eq. (2) can be given as

$$\mathbf{X}(t)=e^{\mathbf{A}(t-t_{\mathrm{st}})}\mathbf{X}\left(t_{\mathrm{st}}\right)+\int_{t_{\mathrm{st}}}^{t}e^{\mathbf{A}(t-\xi)}\mathbf{B}(\xi)[\mathbf{X}(\xi)-\mathbf{X}(\xi-\tau)]d\xi \tag{3}$$

where t_{st} represents the starting time point.

In the milling process, when the tool is not cutting the workpiece, the milling system is in the free vibration state, and the matrix $\mathbf{B}(t)$ is a zero matrix. On the contrary, when the tool is cutting the workpiece, the milling system is in the forced vibration state, and the coefficient matrix $\mathbf{B}(t)$ is a non-zero matrix. Accordingly, the tooth passing period τ can be divided into free vibration duration t_f and forced vibration duration $\tau-t_f$.

In the free vibration duration t_f, Eq. (3) can be simplified as

$$\mathbf{X}\left(t_1\right)=e^{\mathbf{A}(t_1-t_0)}\mathbf{X}\left(t_0\right)=e^{\mathbf{A}t_f}\mathbf{X}\left(t_0\right) \tag{4}$$

where t_0 and t_1 are the starting and ending instants of free vibration, respectively.

Then, the forced vibration duration $\tau-t_f$ is divided into m equal intervals with the step length $h=\left(\tau-t_f\right)/m$. The corresponding discretized time points are $t_i=t_0+t_f+(i-1)h$, where $i=1,2,\cdots,m+1$. It is supposed that the computation starting time point is t_i, Eq. (3) becomes

$$\mathbf{X}(t)=e^{\mathbf{A}(t-t_i)}\mathbf{X}\left(t_i\right)+\int_{t_i}^{t}e^{\mathbf{A}(t-\xi)}\mathbf{B}(\xi)[\mathbf{X}(\xi)-\mathbf{X}(\xi-\tau)]d\xi \tag{5}$$

Substituting $t=t_{i+2}$ into Eq. (5) leads to

$$\mathbf{X}\left(t_{i+2}\right)=e^{2\mathbf{A}h}\mathbf{X}\left(t_i\right)+\int_{t_i}^{t_{i+2}}e^{\mathbf{A}\left(t_{i+2}-\xi\right)}\mathbf{B}(\xi)[\mathbf{X}(\xi)-\mathbf{X}(\xi-\tau)]d\xi \tag{6}$$

Next, the Simpson 1/3 formula with local discretization error of $O\left(h^5\right)$ is used to approximate the integral term in Eq. (6). The state term $\mathbf{X}\left(t_{i+2}\right)$ thus can be approximated as

$$\begin{aligned}\mathbf{X}\left(t_{i+2}\right)=e^{2\mathbf{A}h}\mathbf{X}\left(t_i\right)+\frac{h}{3}\big[&\mathbf{B}\left(t_{i+2}\right)\left(\mathbf{X}\left(t_{i+2}\right)-\mathbf{X}\left(t_{i+2}-\tau\right)\right)+\\ &4e^{\mathbf{A}h}\mathbf{B}\left(t_{i+1}\right)\left(\mathbf{X}\left(t_{i+1}\right)-\mathbf{X}\left(t_{i+1}-\tau\right)\right)+e^{2\mathbf{A}h}\mathbf{B}\left(t_i\right)\left(\mathbf{X}\left(t_i\right)-\mathbf{X}\left(t_i-\tau\right)\right)\big]\end{aligned} \tag{7}$$

To construct the Floquet transition matrix which is used to evaluate the stability of the milling system, Eq. (7) is further written as

$$\begin{aligned}\mathbf{F}\left(t_i\right)\mathbf{X}\left(t_i\right)+\mathbf{F}\left(t_{i+1}\right)\mathbf{X}\left(t_{i+1}\right)+\mathbf{F}\left(t_{i+2}\right)\mathbf{X}\left(t_{i+2}\right)=&\\ -\frac{h}{3}e^{2\mathbf{A}h}\mathbf{B}\left(t_i\right)\mathbf{X}\left(t_i-\tau\right)-\frac{4h}{3}e^{\mathbf{A}h}\mathbf{B}\left(t_{i+1}\right)\mathbf{X}\left(t_{i+1}-\tau\right)&\\ -\frac{h}{3}\mathbf{B}\left(t_{i+2}\right)\mathbf{X}\left(t_{i+2}-\tau\right)&\end{aligned} \tag{8}$$

where $\mathbf{F}\left(t_i\right)=-e^{2\mathbf{A}h}-\frac{h}{3}e^{2\mathbf{A}h}\mathbf{B}\left(t_i\right)$, $\mathbf{F}\left(t_{i+1}\right)=-\frac{4h}{3}e^{\mathbf{A}h}\mathbf{B}\left(t_{i+1}\right)$, $\mathbf{F}\left(t_{i+2}\right)=\mathbf{I}-\frac{h}{3}\mathbf{B}\left(t_{i+2}\right)$.

In addition, t_{m+1} is the ending instant of forced vibration, and $t_{m+1}-\tau=t_0$. Equation (4) can be rewritten as

$$\mathbf{X}\left(t_1\right)=e^{\mathbf{A}t_f}\mathbf{X}\left(t_{m+1}-\tau\right) \tag{9}$$

We first consider only using the Simpson 1/3 formula to construct the Floquet transition matrix. For the convenience of description, $\mathbf{F}\left(t_i\right)$ and $\mathbf{B}\left(t_i\right)$ are abbreviated as $\mathbf{F}_i$ and $\mathbf{B}_i$. By combining Eqs. (8) and (9), a linear discrete map is defined as

$$\mathbf{P}_1\begin{bmatrix}\mathbf{X}\left(t_1\right)\\ \mathbf{X}\left(t_2\right)\\ \vdots\\ \mathbf{X}\left(t_{m+1}\right)\end{bmatrix}_{(2mn+2n)\times 1}=\mathbf{Q}_1\begin{bmatrix}\mathbf{X}\left(t_1-\tau\right)\\ \mathbf{X}\left(t_2-\tau\right)\\ \vdots\\ \mathbf{X}\left(t_{m+1}-\tau\right)\end{bmatrix}_{(2mn+2n)\times 1} \tag{10}$$

with

$$\mathbf{P}_1=\begin{bmatrix}\mathbf{I} & & & & & & \\ \mathbf{F}_1 & \mathbf{F}_2 & \mathbf{F}_3 & & & & \\ & \mathbf{F}_2 & \mathbf{F}_3 & \mathbf{F}_4 & & & \\ & & \mathbf{F}_3 & \mathbf{F}_4 & \mathbf{F}_5 & & \\ & & & \ddots & \ddots & \ddots & \\ & & & & \mathbf{F}_{m-1} & \mathbf{F}_m & \mathbf{F}_{m+1}\end{bmatrix}_{2mn\times(2mn+2n)} \tag{11}$$

$$\mathbf{Q}_1=\begin{bmatrix} -\frac{h}{3}e^{2\mathbf{A}h}\mathbf{B}_1 & -\frac{4h}{3}e^{\mathbf{A}h}\mathbf{B}_2 & -\frac{h}{3}\mathbf{B}_3 & & & & e^{\mathbf{A}t_f}\\ & -\frac{h}{3}e^{2\mathbf{A}h}\mathbf{B}_2 & -\frac{4h}{3}e^{\mathbf{A}h}\mathbf{B}_3 & -\frac{h}{3}\mathbf{B}_4 & & & \\ & & -\frac{h}{3}e^{2\mathbf{A}h}\mathbf{B}_2 & -\frac{4h}{3}e^{\mathbf{A}h}\mathbf{B}_3 & -\frac{h}{3}\mathbf{B}_4 & & \\ & & & \ddots & \ddots & \ddots & \\ & & & & -\frac{h}{3}e^{2\mathbf{A}h}\mathbf{B}_{m-1} & -\frac{4h}{3}e^{\mathbf{A}h}\mathbf{B}_m & -\frac{h}{3}\mathbf{B}_{m+1} \end{bmatrix}_{2mn\times(2mn+2n)} \tag{12}$$

where subscript n denotes the number of degrees of freedom (DOF) of the milling system.

Note that $\mathbf{P}_1$ and $\mathbf{Q}_1$ are not square matrices. In order to obtain the Floquet transition matrix $\mathbf{\Phi}$, one can pre-multiply both sides of the Eq. (10) by the transpose of $\mathbf{P}_1$ or $\mathbf{Q}_1$. For example:

$$\Phi=\left(\mathbf{P}_1^T\mathbf{P}_1\right)^{-1}\left(\mathbf{P}_1^T\mathbf{Q}_1\right) \tag{13}$$

It can be inferred from Eq. (13) that the current Floquet transition matrix construction process will involve a huge amount of multiplications in the program. The Simpson method [29] and some other methods [25, 26] adopt the trapezoidal formula to approximate the second state term $\mathbf{X}(t_2)$, resulting in added rows in the matrices $\mathbf{P}_1$ and $\mathbf{Q}_1$, which makes $\mathbf{P}_1$ and $\mathbf{Q}_1$ become square matrices. This allows the construction of the Floquet transition matrix without the need to pre-multiply the transpose of $\mathbf{P}_1$ or $\mathbf{Q}_1$. Unfortunately, this reduces the order of local discretization error into $O(h^3)$.

$$\mathbf{Q}_2=\begin{bmatrix} -\frac{h}{3}e^{2\mathbf{A}h}\mathbf{B}_1 & -\frac{4h}{3}e^{\mathbf{A}h}\mathbf{B}_2 & -\frac{h}{3}\mathbf{B}_3 & & & & e^{\mathbf{A}t_f}\\ -\frac{3h}{8}e^{3\mathbf{A}h}\mathbf{B}_1 & -\frac{9h}{8}e^{2\mathbf{A}h}\mathbf{B}_2 & -\frac{9h}{8}e^{\mathbf{A}h}\mathbf{B}_3 & -\frac{3h}{8}\mathbf{B}_4 & & & \\ & -\frac{h}{3}e^{2\mathbf{A}h}\mathbf{B}_2 & -\frac{4h}{3}e^{\mathbf{A}h}\mathbf{B}_3 & -\frac{h}{3}\mathbf{B}_4 & & & \\ & & \ddots & \ddots & \ddots & & \\ & & & -\frac{h}{3}e^{2\mathbf{A}h}\mathbf{B}_{m-1} & -\frac{4h}{3}e^{\mathbf{A}h}\mathbf{B}_m & -\frac{h}{3}\mathbf{B}_{m+1} & \end{bmatrix}_{(2mn+2n)\times(2mn+2n)} \tag{18}$$

In order to maintain the fifth-order algorithm accuracy of $(O(h^5))$, apart from the use of 1/3 Simpson formula to approximate most integral terms on each time interval over the forced vibration duration, the hybrid multi-step method proposed in this paper utilizes the 3/8 Simpson formula to approximate the fourth state term $\mathbf{X}(t_4)$ as follows:

$$\mathbf{X}(t_4)=e^{3\mathbf{A}h}\mathbf{X}(t_1)+\frac{3h}{8}\begin{bmatrix}\mathbf{B}_4\left(\mathbf{X}(t_4)-\mathbf{X}(t_4-\tau)\right)+3e^{\mathbf{A}h}\mathbf{B}_3\left(\mathbf{X}(t_3)-\mathbf{X}(t_3-\tau)\right)+3e^{2\mathbf{A}h}\mathbf{B}_2\left(\mathbf{X}(t_2)-\mathbf{X}(t_2-\tau)\right)\\ +e^{3\mathbf{A}h}\mathbf{B}_1\left(\mathbf{X}(t_1)-\mathbf{X}(t_1-\tau)\right)\end{bmatrix} \tag{14}$$

After rearranging Eq. (14), the following relationship can be obtained:

$$\begin{aligned}\mathbf{L}(t_1)\mathbf{X}(t_1)+\mathbf{L}(t_2)\mathbf{X}(t_2)+\mathbf{L}(t_3)\mathbf{X}(t_3)+\mathbf{L}(t_4)\mathbf{X}(t_4)=&-\frac{3h}{8}e^{3\mathbf{A}h}\mathbf{B}_1\mathbf{X}(t_1-\tau)-\frac{9h}{8}e^{2\mathbf{A}h}\mathbf{B}_2(t_2-\tau)\\&-\frac{9h}{8}e^{\mathbf{A}h}\mathbf{B}_3(t_3-\tau)-\frac{3h}{8}\mathbf{B}_4(t_4-\tau)\end{aligned} \tag{15}$$

where $\mathbf{L}(t_1)=-e^{3\mathbf{A}h}-\frac{3h}{8}e^{3\mathbf{A}h}\mathbf{B}_1$, $\mathbf{L}(t_2)=-\frac{9h}{8}e^{2\mathbf{A}h}\mathbf{B}_2$, $\mathbf{L}(t_3)=-\frac{9h}{8}e^{\mathbf{A}h}\mathbf{B}_3$, $\mathbf{L}(t_4)=\mathbf{I}-\frac{3h}{8}\mathbf{B}_4$.

By combining Eqs. (8), (9) and (15), a linear discrete map is defined as

$$\mathbf{P}_2\begin{bmatrix}\mathbf{X}(t_1)\\ \mathbf{X}(t_2)\\ \vdots\\ \mathbf{X}(t_{m+1})\end{bmatrix}_{(2mn+2n)\times1}=\mathbf{Q}_2\begin{bmatrix}\mathbf{X}(t_1-\tau)\\ \mathbf{X}(t_2-\tau)\\ \vdots\\ \mathbf{X}(t_{m+1}-\tau)\end{bmatrix}_{(2mn+2n)\times1} \tag{16}$$

with

$$\mathbf{P}_2=\begin{bmatrix}\mathbf{I} & & & & & \\ \mathbf{F}_1 & \mathbf{F}_2 & \mathbf{F}_3 & & & \\ \mathbf{L}_1 & \mathbf{L}_2 & \mathbf{L}_3 & \mathbf{L}_4 & & \\ & \mathbf{F}_2 & \mathbf{F}_3 & \mathbf{F}_4 & & \\ & & \ddots & \ddots & \ddots & \\ & & & \mathbf{F}_{m-1} & \mathbf{F}_m & \mathbf{F}_{m+1}\end{bmatrix}_{(2mn+2n)\times(2mn+2n)} \tag{17}$$

The Floquet transition matrix $\mathbf{\Phi}$ thus can be expressed as

$$\Phi=\left(\mathbf{P}_2\right)^{-1}\mathbf{Q}_2 \tag{19}$$

Comparing Eq. (13) with Eq. (19), it can be seen that the number of multiplications will be greatly reduced during the computation of the transfer matrix $\mathbf{\Phi}$.

Table 1 System parameters of 1 DOF model

f_n (Hz)	ξ	m_t (kg)	K_t (N/mm^2)	K_n (N/mm^2)	N
922	0.011	0.03993	600	200	2

Finally, according to Floquet theory, if the modules of all the eigenvalues of $\mathbf{\Phi}$ are less than 1, the milling process can be determined to be stable; otherwise, unstable.

3 Numerical verification

A single DOF milling example from Ref. [36] is adopted in this section to evaluate the convergence rate and computation efficiency of the proposed method. The system parameters are listed in Table 1. All programs in this paper are conducted using MATLAB R2020a and ran on a desktop computer with Intel(R) Core (TM) i7-10750H CPU @ 2.60 GHz and 16 GB memory. The milling dynamics equation in state-space form is the same as Eq. (2), in which $\mathbf{A}$ and $\mathbf{B}(t)$ are expressed as follows:

$$\mathbf{A}=\begin{bmatrix} -\xi\omega_n & \frac{1}{m_t} \\ m_t\left(\xi\omega_n\right)^2-m_t\omega_n^2 & -\xi\omega_n \end{bmatrix},\mathbf{B}(t)=\begin{bmatrix} 0 & 0 \\ -a_p h(t) & 0 \end{bmatrix} \tag{20}$$

where

$$h(t)=\sum_{j=1}^{N} g\left(\varphi_j(t)\right)\sin\left(\varphi_j(t)\right)\left[K_t\cos\left(\varphi_j(t)\right)+K_n\sin\left(\varphi_j(t)\right)\right] \tag{21}$$

where $\varphi_j(t)$ represents the angular position of tooth j. K_t and K_n represent the tangential and normal cutting force coefficients, respectively. $g\left(\varphi_j(t)\right)$ is a window function, which equals to 1 when the cutter is in cut and otherwise equals to 0.

3.1 Rate of convergence analysis

The local discretization error is defined as the absolute value deviation between $|\mu|$ and $|\mu_0|$, where $|\mu|$ is the approximate critical eigenvalue of the Floquet transition matrix and $|\mu_0|$ is the exact critical eigenvalue. In order to evaluate the convergence performance more comprehensively, both large and small radial immersion conditions are examined. The milling process with large radial immersion is first examined. The corresponding cutting parameters are as follows: down-milling, spindle speed $\Omega=10{,}000$ rpm, radial immersion ratio $a/D=1$, and depths of cut $a_p=0.5$, 1, 1.5, and 2 mm. Figure 1 shows the convergence curves of the UNIM, the 4th FMD, the 2nd SDM, and the proposed method. The exact critical eigenvalue $|\mu_0|$ is obtained using the UNIM with $m=400$. It can be easily seen that the proposed method converges much faster than

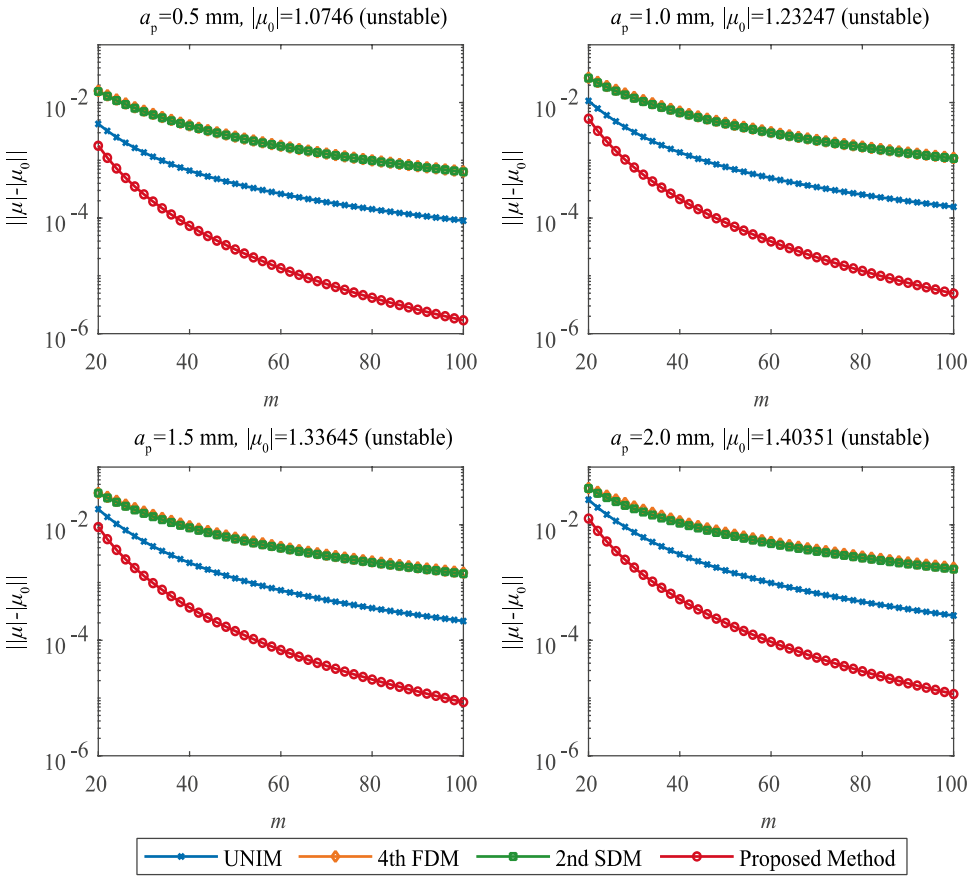

Fig. 1 Convergence curves of the UNIM, 4th FMD, the 2nd SDM, and the proposed method with $a/D=1$ and $\Omega=10{,}000$ rpm

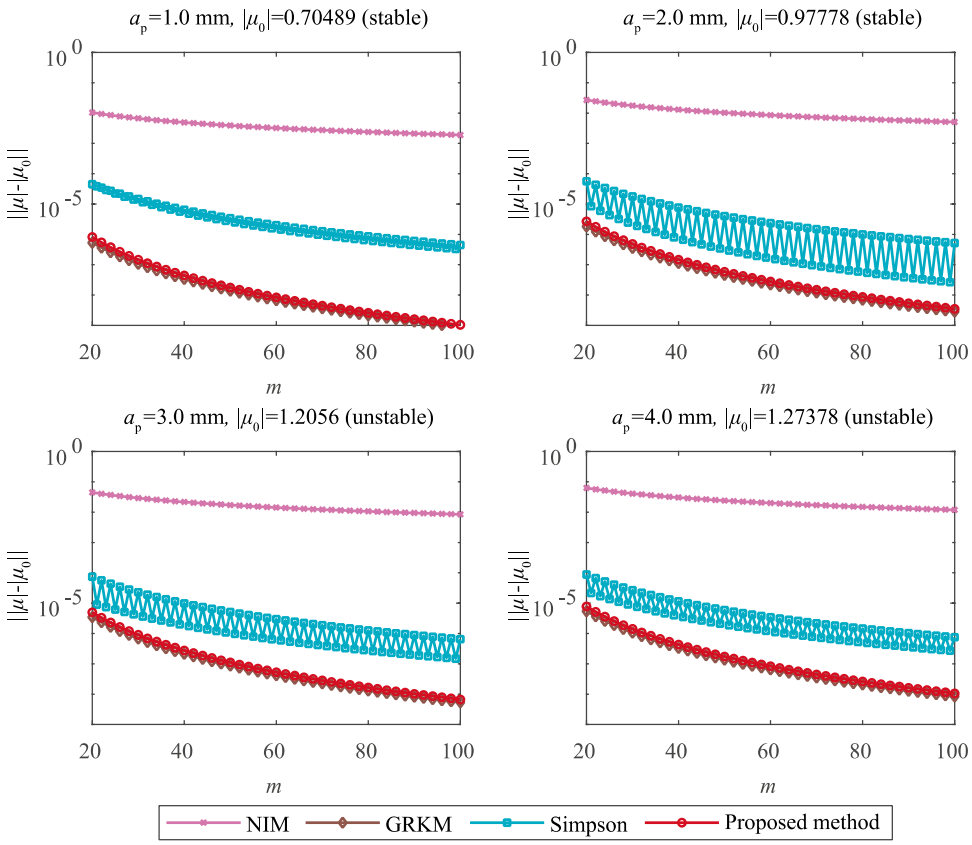

Fig. 2 Convergence curves of the NIM, the GRKM, the Simpson method, and the proposed method with $a/D=0.05$ and $\Omega=8000$ rpm

the other three methods. In order to evaluate the convergence rate of the proposed method under small immersion conditions, some methods whose convergence performance has been proved to be good under such conditions are compared, including the NIM, the GRKM, and the Simpson method. The corresponding cutting parameters are as follows: $\Omega=8000$ rpm, a/D = 0.05, $a_p=1$, 2, 3, and 2 mm. The convergence curves of the NIM, the GRKM, the Simpson method, and the proposed method are shown in Fig. 2. The exact value $|\mu_0|$ is now also determined by the GRKM with $m=400$. It can be seen that under small immersion conditions, the convergence rate of the proposed method obviously outweighs the NIM and the Simpson method. Even compared with highly convergent GRKM, the proposed method can also achieve the same order of convergence with only a very slight disadvantage.

3.2 Comparison of stability lobe diagrams

From SDMs and FDMs that are the most used methods for milling stability predictions in the discrete time domain, the 1st SDM and 4th FDM are selected respectively to compare with the proposed method in terms of computational efficiency and accuracy. Based on the single DOF milling system, the SLDs are determined by the 1st SDM, 4th FDM, and the proposed method.

Figure 3 shows the SLDs for the single DOF milling model with $a/D=1$ and discretization number $m=40$, 60. In Fig. 3, the reference SLD with the red dotted line is obtained by the 4th FDM with $m=200$. The SLDs are constructed over a 200×100 sized grid. The spindle speed Ω ranges from 5 to 10 krpm, and the axial depth of cut a_p ranges from 0 to 10 mm. It can be seen from Fig. 3 that the proposed method is significantly more accurate than the 1st SDM. In Ref. [23], it had proved that the 4th FDM can be used to predict the so-called lobbing effect well. However, it can be seen obviously from the enlargements in Fig. 3 that the proposed method gives a more accurate prediction than the 4th FDM. The above two points mean that under large immersion conditions, the proposed method has higher computational accuracy than the 1st SDM and the 4th FDM. Another observation from Fig. 3 is that the proposed method consumes less computation time than the 1st SDM and the 4th FDM with the same m. For example, when $m=40$, the 1st SDM and the 4th FDM take 114 s and 32 s, but the proposed method takes only 16 s. This indicates that the computation time of the proposed method can be reduced by around 86% and 50% compared with the 1st SDM and the 4th FDM.

The performance of the proposed method under small radial immersion conditions is also investigated. Here, m

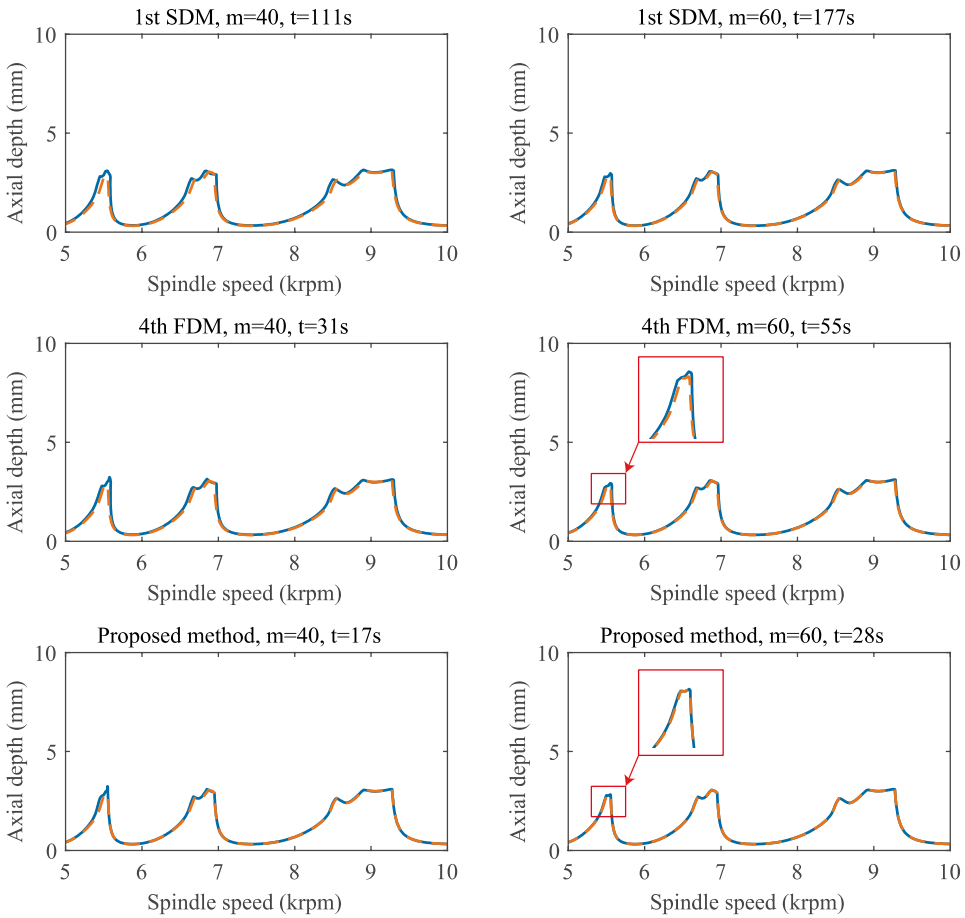

Fig. 3 SLDs obtained by the 1st SDM, 4th FDM, and the proposed method with $a/D = 1$

is respectively set as 20 and 40. The reference SLD with the red dotted line is also obtained by the 4th FDM with $m = 200$. The two parameters Ω and a_p range remain the same, and a/D is set as 0.05. Figure 4 shows the SLDs predicted by 1st SDM, 4th FDM, and the proposed method. It can be also observed that the proposed method also achieves higher computational accuracy and efficiency than the 1st SDM and the 4th FDM under small radial immersion conditions.

4 Experiment verification

To verify the reliability and feasibility of the proposed method, a series of cutting tests are carried on a five-axis milling machine center DMU60. A four-flute flat-end cutter with 20 mm diameter is used in all the cutting tests. The workpiece (Aluminum 7075-T6) is mounted on a single-degree-of-freedom fixture to ensure that the variation of modal parameters caused by material removal can be ignored during the machining operations, as shown in Fig. 5. In the cutting tests, the displacements and the sound signals are collected at the same time. Specifically, a non-contact eddy current displacement sensor is used to measure the workpiece vibrations and a microphone is used to measure the sound pressure.

Before cutting tests, the modal parameters of the flexible workpiece-fixture system are identified by impact hammer tests. A PCB 086C01 impact hammer with a piezoelectric force transducer is used to excite the workpiece and the resulting response signals are collected by a PCB 356A01 accelerometer. The frequency response function (FRF) is recorded by the LMS data acquisition system. The modal parameters are identified using the rational fraction polynomial algorithm [37]: the natural frequency $\omega_n = 250.336$ rad/s, the damping ratio $\xi = 0.00155$, and the modal mass $m_t = 1.897$ kg. Figure 6a shows the measured FRF and the fitted FRF curves.

Slot milling experiments are conducted to calibrate the cutting force coefficients. In the calibration experiments, the spindle speed and axial depth of cut remain constant, and the feed per tooth varies from 0.025 to 0.075 mm/tooth. Then the cutting force coefficients can be determined by the widely used linear regression approach. Figure 6b shows the linear regression results of average milling forces respectively in X, Y, and Z directions as functions of feed per tooth. The

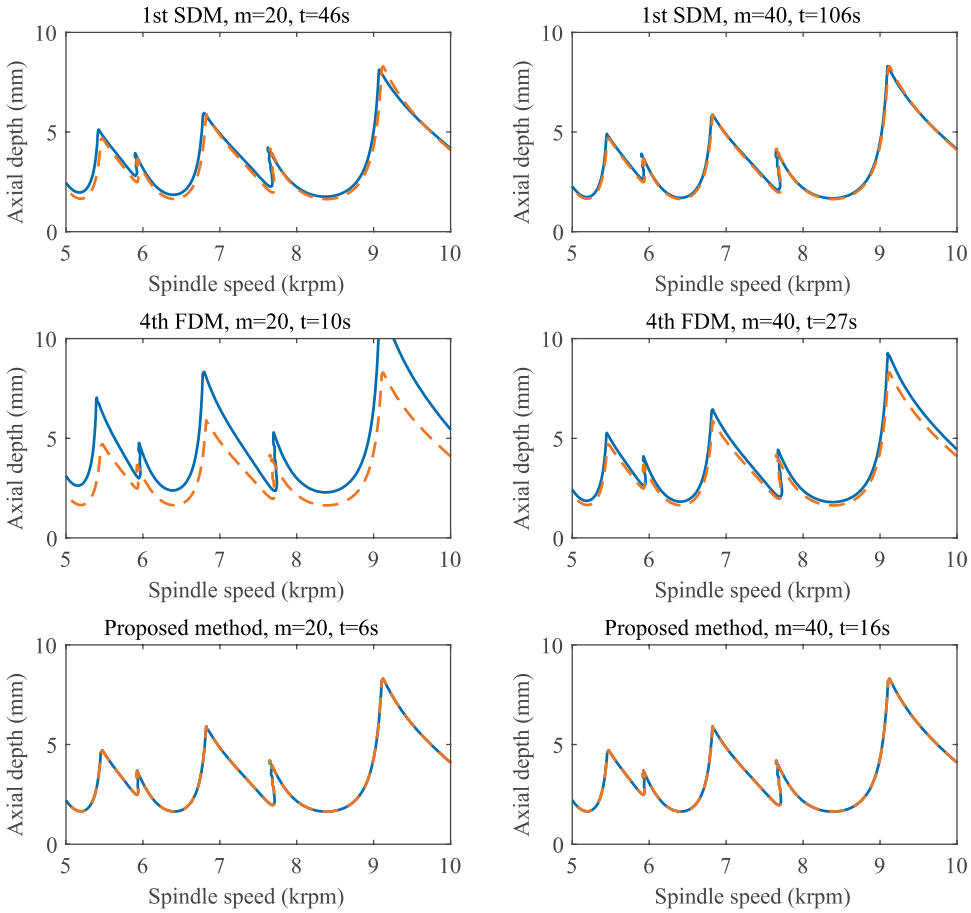

Fig. 4 SLDs obtained by the 1st SDM, 4th FDM, and the proposed method with $a/D = 0.05$

identified tangential and radial cutting force coefficients are 911.72 N/mm^2 and 201.44 N/mm^2.

Based on the identified modal parameters and cutting force coefficients, the SLD is drawn with the proposed method for a down-milling operation with the radial depth of cut 0.6 mm, as shown in Fig. 7. The black line in Fig. 7 represents the stability lobe borders. Generally, the upper part of it represents the unstable cutting parameter space, and the lower part of it represents the stable cutting parameter space. In order to verify the accuracy of the predicted SLD, a series of down-milling experiments with different spindles and axial depths of cut are carried out. The machining parameters are listed in Table 2.

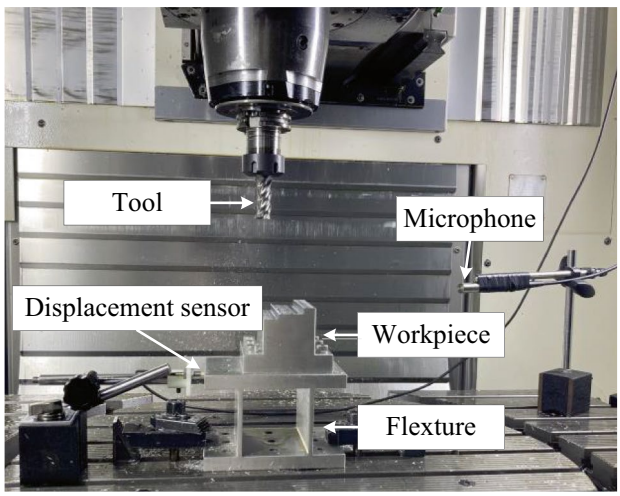

Fig. 5 Experimental setup

To realize the accurate judgment of the actual cutting state, the displacements and sound signals collected during the machining process should be analyzed. These signals are converted from the time domain into the frequency domain via the fast Fourier transformation (FFT), and whether the cutting process is stable or not can be distinguished from the displacement spectra or sound spectra. The process is identified as stable if the peaks in the frequency spectra appear at integer multiples of tooth passing and spindle rotation frequencies. Otherwise, it is unstable if the frequency spectra have peaks around the natural frequencies of workpiece or tool, and the amplitudes at peak frequencies are roughly equal or exceed the amplitudes at tooth passing and spindle rotation frequencies. By means of the above analysis method, the experimentally observed stability results are plotted in Fig. 7, where the circles and the crosses represent the stable and unstable milling state, respectively. It can be

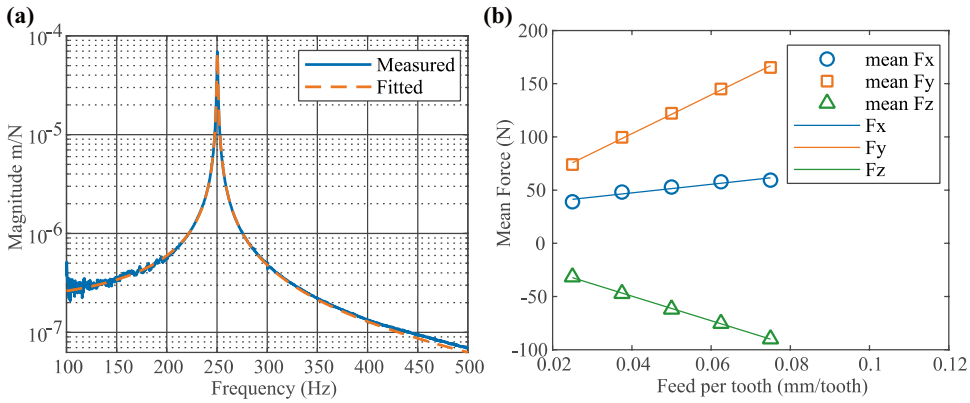

Fig. 6 (**a**) The measured and fitted FRF curves of the flexible workpiece-fixture system and (**b**) linear regression results

seen that the actual cutting test results are in good agreement with the predicted stability lobe borders.

Figures 8, 9 and 10 show the displacements and sound signals of some cutting tests together with their frequency spectra. The sound signals and the workpiece surface textures of point A (3400 rpm, 3 mm) and point B (4000 rpm, 3 mm) are shown in Fig. 8. It is seen from Fig. 8 that the peaks in the sound spectrum of the point A only appear at tooth passing frequency (3400/60*4 ≈ 226.7 Hz). In addition, the finished surface is relatively smooth, which implies that the cutting process is stable. However, the sound spectrum of the point B shows that the chatter frequency is 253.5 Hz, which is close to the natural frequency of the workpiece, and its amplitude is much larger than the amplitude at the frequency of two times tooth pass frequency (2*4000/60*4 ≈ 2*266.7 ≈ 533.5 Hz). It can be seen that there are obvious chatter marks on the finished surface.

It is worth noting that a red unstable lobe is also drawn in Fig. 7, and it represents the contour line when the eigenvalue is 1.2. Theoretically, if the calculated eigenvalue at the selected parameter point is larger, it indicates that the point is more unstable, and the time domain amplitude of the signal and peak value of the frequency spectrum will be larger. Figure 9 shows the sound signals collected together with their frequency spectra when the machining parameter combinations are points C (1800 rpm, 4 mm), D (1900 rpm, 4 mm), and E (2000 rpm, 4 mm). In the time domain, when the machining parameter combination changes from point C to point E (i.e., the spindle speed changes from 1800 to 1900 rpm, and then to 2000 rpm), the time domain intensity of the sound signal gradually increases; in the frequency spectrum, there are only the tooth pass frequency (1800/60*4 = 120 Hz) and its second harmonic frequency (120*2 = 240 Hz) for point C, which means that the point C is stable. For points D and E, chatter frequencies are respectively 253.5 Hz and 255 Hz, which stands for points D and E are unstable. Another observation from Fig. 9 is that the peak value of the frequency spectrum of point E is significantly greater than that of point D. This is very consistent with the fact that the eigenvalue

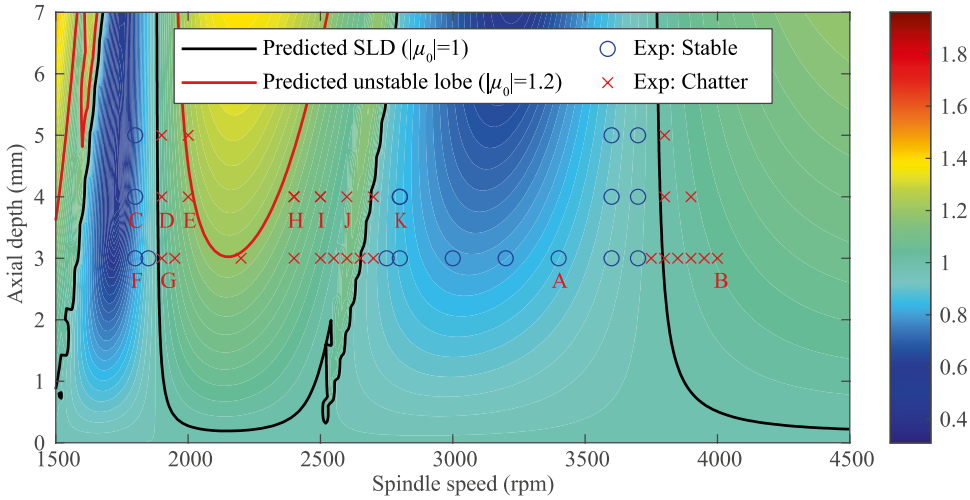

Fig. 7 Predicted SLD with the proposed method

Table 2 The machining parameters of down-milling experiments

No.	Spindle speed (rpm)	Axial depth (mm)	Radial depth (mm)	Feed peer tooth (mm)
1–6	1800, 1850, 1900, 1950, 2200, 2400	3	0.6	0.05
7–12	2500, 2550, 2600, 2650, 2700, 2750	3	0.6	0.05
13–18	2800, 3000, 3200, 3400, 3600, 3700	3	0.6	0.05
19–24	3750, 3800, 3850, 3900, 3950, 4000	3	0.6	0.05
25–30	1800, 1900, 2000, 2400, 2500, 2600	4	0.6	0.05
31–36	2700, 2800, 3600, 3700, 3800, 3900	4	0.6	0.05
37–42	1800, 1900, 2000, 3600, 3700, 3800	5	0.6	0.05

of point E is close to 1.2, closing to the red contour, while the eigenvalue of point D is close to 1. In addition, this can also be seen from the color change of the color map in Fig. 7.

Figure 10 shows the measured sound and displacement signals of the selected parameter points F–H and their corresponding frequency spectra. It can be seen that by analyzing the time domain waveforms and frequency spectra of the two different signals, the same stability measurement results can be obtained for the same parameter combinations. The blue line in Fig. 10 represents the sound signals, and the orange line represents the displacement signals. It can be seen that if the time domain amplitudes of these sound signals are observed separately, the point G (1900 rpm, 4 mm) can be determined to be unstable (chatter) due to relatively large time domain amplitude. Similarly, it can also be identified that the point F (1800 rpm, 3 mm) is stable, and its waveform is smooth with a relatively small amplitude. On the other hand, in the sound frequency spectrum of point F, only tooth passing frequency (1800/60*4 = 120 Hz) and its second harmonic frequency (240 Hz) appear; in the sound frequency spectrum of point G, it can be seen that chatter frequency is 253.5 Hz. As for whether every point H (2400 rpm, 4 mm), I (2500 rpm, 4 mm), J (2600 rpm, 4 mm), and K (2800 rpm, 4 mm) is stable or unstable, it requires further analysis of the frequency spectra of the corresponding sound signals. Chatter frequencies of 269 Hz, 274 Hz, and 279 Hz are observed in the sound frequency spectra of points H, I, and J, and their amplitudes are all greater than the corresponding tooth pass frequencies (2400/60*4 = 160 Hz, 2500/60*4 = 166.6 Hz, 2600/60*4 = 173.3 Hz), which means that points H, I, and J are all unstable. However, for point K, the sound frequency spectrum shows that there are tooth pass frequency (2800/60*4 = 186.7 Hz) and its second harmonic frequency (2*186.7 = 373.4 Hz), which means that the point K is stable. In addition, analyzing the displacement signals and the corresponding frequency spectra can achieve the same conclusion. The above analysis shows that the proposed method has the ability to accurately predict the stability of the actual milling processes, so it can be used to select appropriate machining parameter combinations to avoid chatter.

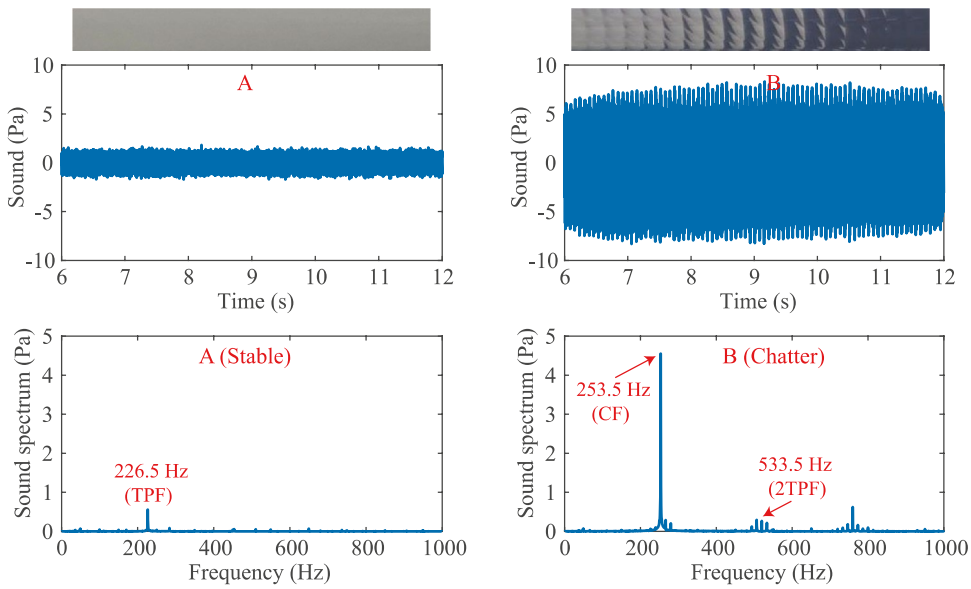

Fig. 8 Surface textures, sound signals, and frequency spectra of points A and B. Here, symbol "CF" means the chatter frequency. "TPF" stands for the tooth passing frequency

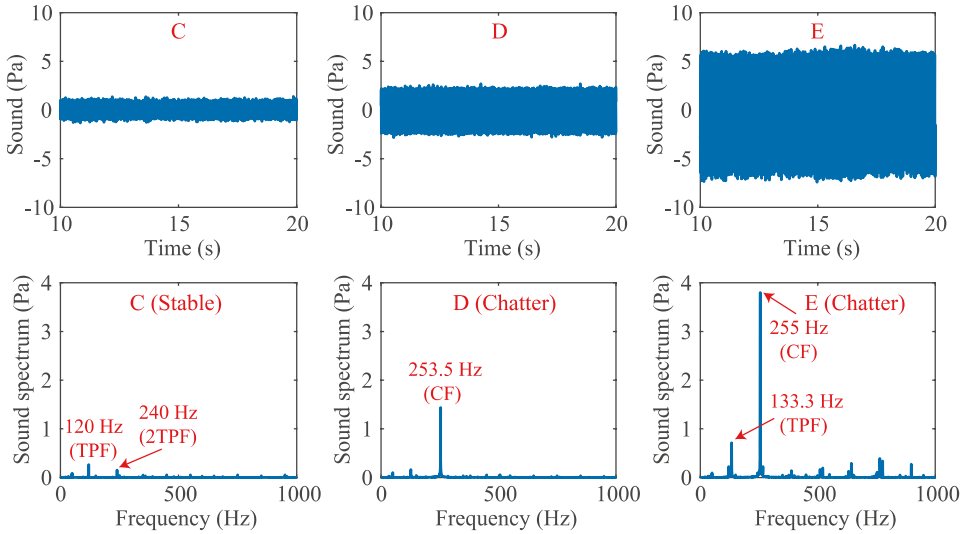

Fig. 9 Sound signals and frequency spectra of points C, D, and E

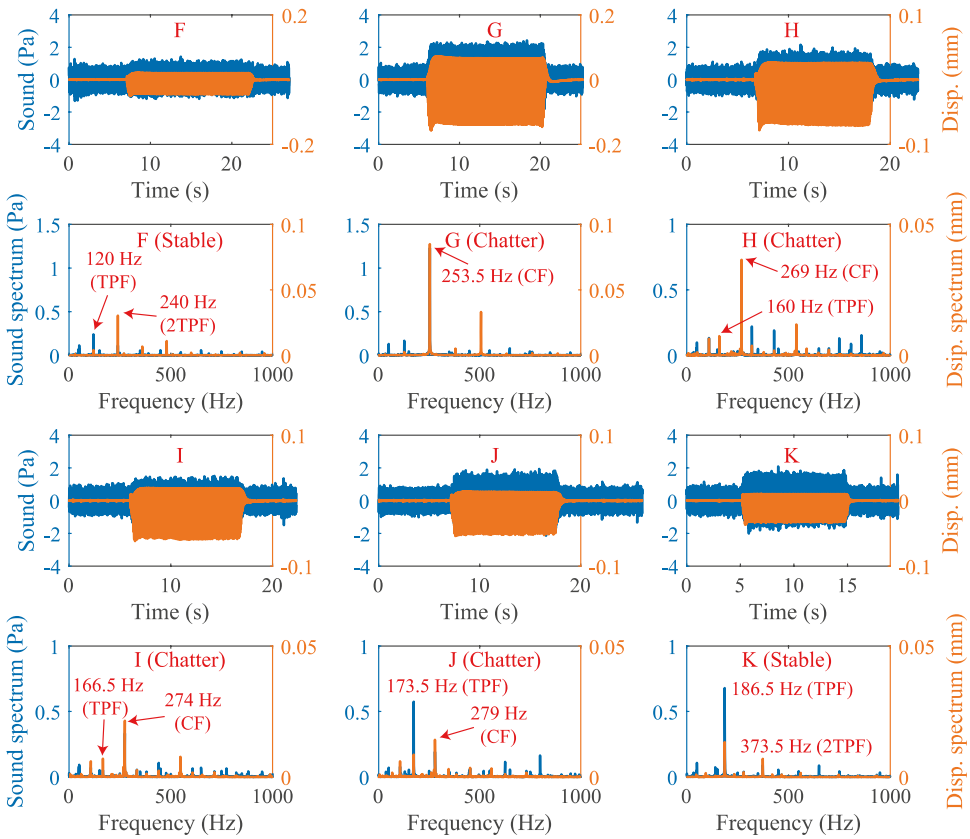

Fig. 10 Sound signals, displacement signals, and frequency spectra of points F, G, H, I, J, and K. Here "Disp." is the abbreviation of "Displacement"

5 Conclusions

In this work, a hybrid multi-step method based on 1/3 and 3/8 Simpson formulas is proposed to predict the milling stability. From this study, some conclusions are summarized as follows:

1. Instead of using the trapezoidal rule to approximate the state term $\mathbf{X}(t_2)$, all the state terms are approximated by the hybrid multi-step method with a fifth-order computational accuracy.
2. Convergence analysis shows that the proposed method has a faster convergence rate than the UNIM, the 4th

FMD, the 2nd SDM, the NIM, and the Simpson method under the same computational parameters.
3. The SLD determined by using the method proposed has a better agreement with the reference SLD than the 1st SDM and the 4th FDM even using smaller discrete steps.
4. To further verify the availability of the proposed method, a series of milling experiments are carried out and lots of sound and displacement signals are analyzed. The experimental results show that the proposed method can accurately predict the stability of the actual milling process.

Author contribution Methodology, investigation, software, writing–original draft: Danian Zhan; methodology, writing–review and editing: Shanglei Jiang; validation, investigation: Shikang Li; writing–review and editing, supervision: Yuwen Sun.

Funding This work was supported by the National Key Research and Development Program of China (Grant No. 2018YFA0704603) and the National Science Foundation of China (Grant No. 91948203).

Data availability Data and materials used in this research are available.

Declarations

Ethics approval This work does not contain any studies with human participants or animals performed by any of the authors.

Consent to participate Not applicable.

Consent to publish All the authors have read and agreed to the published version of the manuscript.

Conflict of interest The authors declare no competing interests.

References

1. Altintas Y, Stepan G, Budak E, Schmitz T, Kilic ZM (2020) Chatter stability of machining operations. J Manuf Sci Eng 142(11):1–46. https://doi.org/10.1115/1.4047391
2. Altintas Y, Stepan G, Merdol D, Dombovari Z (2008) Chatter stability of milling in frequency and discrete time domain. CIRP J Manuf Sci Technol 1(1):35–44. https://doi.org/10.1016/j.cirpj.2008.06.003
3. Yue C, Gao H, Liu X, Liang ST, Wang L (2019) A review of chatter vibration research in milling. Chin J Aeronaut 32(2):215–242. https://doi.org/10.1016/j.cja.2018.11.007
4. Smith S, Tlusty J (1993) Efficient simulation programs for chatter in milling. CIRP Ann 42(1):463–466. https://doi.org/10.1016/S0007-8506(07)62486-X
5. Campomanes ML, Altintas Y (2003) An improved time domain simulation for dynamic milling at small radial immersions. J Manuf Sci Eng 125(3):416–422. https://doi.org/10.1115/1.1580852
6. Altintaş Y, Budak E (1995) Analytical prediction of stability lobes in milling. CIRP Ann 44(1):357–362. https://doi.org/10.1016/S0007-8506(07)62342-7
7. Gradišek J, Kalveram M, Insperger T, Weinert K (2005) On stability prediction for milling. Int J Mach Tools Manuf 45(7–8):769–781. https://doi.org/10.1016/j.ijmachtools.2004.11.015
8. Budak E, Altintas Y (1998) Analytical prediction of chatter stability in milling—part I: general formulation. Trans ASME J Dyn Syst Meas Control 120(1):22–30. https://doi.org/10.1115/1.2801317
9. Merdol SD, Altintas Y (2004) Multi frequency solution of chatter stability for low immersion milling. J Manuf Sci Eng 126(3):459–466. https://doi.org/10.1115/1.1765139
10. Insperger T, Stépán G (2004) Updated semi-discretization method for periodic delay-differential equations with discrete delay. Int J Numer Methods Eng 61(1):117–141. https://doi.org/10.1002/nme.1061
11. Insperger T, Stépán G, Turi J (2008) On the higher-order semidiscretizations for periodic delayed systems. J Sound Vib 313(1–2):334–341. https://doi.org/10.1016/j.jsv.2007.11.040
12. Long XH, Balachandran B, Mann BP (2007) Dynamics of milling processes with variable time delays. Nonlinear Dyn 47:49–63. https://doi.org/10.1007/s11071-006-9058-4
13. Wan M, Zhang WH, Dang JW, Yang Y (2010) A unified stability prediction method for milling process with multiple delays. Int J Mach Tools Manuf 50(1):29–41. https://doi.org/10.1016/j.ijmachtools.2009.09.009
14. Feng J, Wan M, Dong ZY, Zhang WH (2019) A unified process damping model considering the varying stiffness of the milling system. Int J Mach Tools Manuf 147:103470. https://doi.org/10.1016/j.ijmachtools.2019.103470
15. Jiang SL, Sun YW, Yuan XY, Liu WR (2017) A second-order semi-discretization method for the efficient and accurate stability prediction of milling process. Int J Adv Manuf Technol 92(1–4):583–595. https://doi.org/10.1007/s00170-017-0171-y
16. Sun YW, Jiang SL (2018) Predictive modeling of chatter stability considering force-induced deformation effect in milling thin-walled parts. Int J Mach Tools Manuf 135:38–52. https://doi.org/10.1016/j.ijmachtools.2018.08.003
17. Zhan DN, Jiang SL, Niu JB, Sun YW (2020) Dynamics modeling and stability analysis of five-axis ball-end milling system with variable pitch tools. Int J Mech Sci 182:105774. https://doi.org/10.1016/j.ijmecsci.2020.105774
18. Ding Y, Zhu LM, Zhang XJ, Ding H (2010) A full-discretization method for prediction of milling stability. Int J Mach Tools Manuf 50(5):502–509. https://doi.org/10.1016/j.ijmachtools.2010.01.003
19. Ding Y, Zhu LM, Zhang XJ, Ding H (2010) Second-order fulldiscretization method for milling stability prediction. Int J Mach Tools Manuf 50(10):926–932. https://doi.org/10.1016/j.ijmachtools.2010.05.005
20. Guo Q, Sun YW, Jiang Y (2012) On the accurate calculation of milling stability limits using third-order full-discretization method. Int J Mach Tools Manuf 62:61–66. https://doi.org/10.1016/j.ijmachtools.2012.07.008
21. Ozoegwu CG, Omenyi SN (2016) Third-order least squares modelling of milling state term for improved computation of stability boundaries. Prod Manuf Res 4(1):46–64. https://doi.org/10.1080/21693277.2016.1194778
22. Ozoegwu CG, Omenyi SN, Ofochebe SM (2015) Hyper-third order full-discretization methods in milling stability prediction. Int J Mach Tools Manuf 92:1–9. https://doi.org/10.1016/j.ijmachtools.2015.02.007
23. Ozoegwu CG (2016) High order vector numerical integration schemes applied in state space milling stability analysis. Appl Math Comput 273:1025–1040. https://doi.org/10.1016/j.amc.2015.10.069
24. Bayly PV, Mann BP, Schmitz TL, Peters DA, Stepan G, Insperger T (2002) Effects of radial immersion and cutting direction on chatter instability in end-milling. ASME Int Mech Eng Congress Expos 351–363. https://doi.org/10.1115/imece2002-39116
25. Ding Y, Zhu LM, Zhang XJ, Ding H (2011) Numerical integration method for prediction of milling stability. J Manuf Sci Eng 133(3):031005. https://doi.org/10.1115/1.4004136
26. Xia Y, Wan Y, Luo XC, Liu ZQ, Song QH (2021) An improved numerical integration method to predict the milling stability based

on the Lagrange interpolation scheme. Int J Adv Manuf Technol 116(7):2111–2123. https://doi.org/10.1007/s00170-021-07311-z
27. Zhang XJ, Xiong CH, Ding Y, Xiong YL (2011) Variable-step integration method for milling chatter stability prediction with multiple delays. Sci China Technol Sci 54(12):3137–3154. https://doi.org/10.1007/s11431-011-4599-2
28. Niu JB, Ding Y, Zhu LM, Ding H (2014) Runge-Kutta methods for a semi-analytical prediction of milling stability. Nonlinear Dyn 76(1):289–304. https://doi.org/10.1007/s11071-013-1127-x
29. Zhang Z, Li HG, Meng G, Liu C (2015) A novel approach for the prediction of the milling stability based on the Simpson method. Int J Mach Tools Manuf 99:43–47. https://doi.org/10.1016/j.ijmachtools.2015.09.002
30. Dong XF, Qiu ZZ (2020) Stability analysis in milling process based on updated numerical integration method. Mech Syst Signal Process 137:106435. https://doi.org/10.1016/j.ymssp.2019.106435
31. Li WT, Wang LP, Yu G (2020) An accurate and fast milling stability prediction approach based on the Newton-Cotes rules. Int J Mech Sci 177:105469. https://doi.org/10.1016/j.ijmecsci.2020.105469
32. Wang LP, Li WT, Yu G (2022) Time domain study on the construction mechanism of milling stability lobe diagrams with multiple modes. J Manuf Sci Eng 144(2):021007. https://doi.org/10.1115/1.4051794
33. Ding Y, Zhu LM, Zhang XJ, Ding H (2013) Stability analysis of milling via the differential quadrature method. J Manuf Sci Eng 135(4):044502. https://doi.org/10.1115/1.4024539
34. Qin CJ, Tao JF, Shi HT, Xiao DY, Li BC, Liu CL (2020) A novel Chebyshev-wavelet-based approach for accurate and fast prediction of milling stability. Precis Eng 62:244–255. https://doi.org/10.1016/j.precisioneng.2019.11.016
35. Altintas Y, Weck M (2004) Chatter stability of metal cutting and grinding. CIRP Ann 53(2):619–642. https://doi.org/10.1016/S0007-8506(07)60032-8
36. Insperger T (2010) Full-discretization and semi-discretization for milling stability prediction: some comments. Int J Mach Tools Manuf 50(7):658–662. https://doi.org/10.1016/j.ijmachtools.2010.03.010
37. Richardson MH, Formenti DL (1982) Parameter estimation from frequency response measurements using rational fraction polynomials. Proc 1st Int Modal Anal Conf 167–186